Decay of the compound nucleus $^{297}118^*$ formed in the reaction $^{249}Cf + ^{48}Ca$ using the dynamical cluster-decay model

Gudveen Sawhney,[1,*] Amandeep Kaur,[2] Manoj K. Sharma,[2] and Raj K. Gupta[1]
[1]*Department of Physics, Panjab University, Chandigarh 160014, India*
[2]*School of Physics and Materials Science, Thapar University, Patiala 147004, India*
(Received 4 October 2015; published 7 December 2015)

The decay of the $Z = 118$, $^{297}118^*$ compound system, formed in the $^{249}Cf + ^{48}Ca$ reaction, is studied for $2n$, $3n$, and $4n$ emissions, by using the dynamical cluster-decay model (DCM) at compound-nucleus (CN) excitation energies $E^*_{CN} = 29.2$ and 34.4 MeV. A parallel attempt is made to analyze the $^{294}118$ residue nucleus synthesized in the $^{250}Cf + ^{48}Ca$ reaction, subsequent to the $4n$ emission from the $^{298}118^*$ nucleus, to check the possibility of isotopic mixing in the ^{249}Cf target used in the $^{249}Cf + ^{48}Ca$ reaction. The possible role of deformations and orientations, together with different nuclear proximity potentials, is also investigated. In addition, an exclusive analysis of the mass distributions of $Z = 113$ to 118 superheavy nuclei, formed in ^{48}Ca-induced reactions, is explored within the DCM. A comparative importance of Prox-1977 and Prox-2000 potentials on the α-decay chains is also investigated, first by using the preformed cluster model (PCM) for spontaneous decays ($T = 0$), the PCM($T = 0$), and then analyzing the possible role of excitation energy in PCM, i.e., PCM($T \neq 0$), via the measured recoil energy of the residual $^{294}118$ nucleus left after $3n$ emission from $^{297}118^*$ CN. The branching of α decay to the most-probable clusters is also examined for $^{294}118^*$ and its subsequent $^{290}116^*$ and $^{286}114^*$ parents occurring in the α-decay chain. Interestingly, the calculated decay half-lives for some clusters such as ^{86}Kr, ^{84}Se, and ^{80}Ge, referring to doubly magic ^{208}Pb or its neighboring daughter nucleus, present themselves as exciting new possibilities, though to date difficult to observe, of heavy cluster emissions in superheavy mass region.

DOI: 10.1103/PhysRevC.92.064303 PACS number(s): 25.70.Gh, 27.90.+b, 23.60.+e, 23.70.+j

I. INTRODUCTION

In recent years, the synthesis of superheavy elements (SHEs) has emerged as an important research area and a number of isotopes of nuclei having atomic numbers up to $Z = 118$, exhibiting half-lives as long as a few seconds, have been observed either as cold-fusion reactions with ^{208}Pb or ^{209}Bi as the target [1–3] or as hot-fusion ones induced by ^{48}Ca projectiles [4–7]. In all of these reactions, formed by the complete fusion process, the residual superheavy nucleus (SHN) formed after the evaporation of x neutrons has a relatively longer life and decay primarily through consecutive α emissions, eventually terminated either by a known α-decaying or spontaneous-fissioning nucleus. Another decay channel for the excited compound system is that of light-particles (LPs: n, p, α, γ) emission, the evaporation residue (ER), the fusion-fission (FF) process, and the noncompound nucleus decay, which has also been of similar interest (see, e.g., the schematically illustrated Fig. 1 in Ref. [8]). Note that, even though new experiments are presently running at various laboratories and attempts to produce $Z = 120$ are reported [9], the heaviest element known to date is $Z = 118$. The low probability of formation and the separation of short-lived compound nucleus from the very high flux of incident projectile nuclei, can be quoted as the main experimental difficulty in identifying the new SHN. Despite significant developments, both in theory and in experimental facilities, still there are numerous unanswered questions related to this island of stability of SHEs.

Experimentally, the recent synthesis of $Z = 118$ element has been carried out at Joint Institute for Nuclear Research in Dubna, Russia [6,7], to investigate the $3n$ evaporation channel of $^{297}118^*$ compound nucleus (CN) in $^{249}Cf + ^{48}Ca$ complete fusion reaction at CN excitation energies $E^*_{CN} = 29.2 \pm 2.5$ and 34.4 ± 2.3 MeV ($E_{beam} = 245$ and 251 MeV, respectively). In addition, only an upper limit of $2n$ ER cross section, i.e., $\sigma_{2n} \leqslant 0.9$ pb, has been observed [7] at 34.4 ± 2.3 MeV (no decay chain of $^{295}118$ isotope has been observed). The target used in these experiments [7] was >98% enriched isotope ^{249}Cf. This data on $3n$-emission cross section σ_{3n} at two E^*_{CN}'s could not be explained on a theoretical model [10] based on the concept of a dinuclear system (DNS) involving a competition between the quasifission and CN formation processes, because it required an inevitable presence of ^{250}Cf isotope in the nearly enriched ^{249}Cf target, i.e., the observed $^{294}118$ residue cross sections at the two different beam energies [7] are contributed by $3n$ emission from $^{297}118^*$ and $4n$ emission from $^{298}118^*$ compound systems. Extending the idea of isotope-mixed targets further, some other authors [11,12] have predicted the excitation functions of xn-emission cross sections for $^{249–252}Cf$ targets bombarded with ^{48}Ca beam. In the present paper, we show that our interpretation of the observed data on the xn evaporation channel of $^{297}118^*$ CN, based on the dynamical cluster-decay model (DCM), is adequate for a pure ^{249}Cf target and predict cross sections of similar order for the, not yet used, ^{250}Cf target.

The first attempt to synthesize $Z = 118$ was undertaken at Berkeley [13], using the cold-fusion reaction $^{208}Pb(^{86}Kr, 1n)^{293}118$, which resulted in a very high fusion cross section ($2.2^{+2.6}_{-0.8}$ pb), compared to the limiting value of $\sim$1 pb for other cold-fusion reactions up to $Z = 112$, and

*gudveen.sahni@gmail.com

hence the observed α-decay chain of residue nucleus $^{293}118$ was later retracted because the data could not be reproduced in many subsequent experiments at Berkeley and around the world. At about the same time, using their preformed cluster model (PCM), Gupta and collaborators [14] analyzed the nuclear structure effects in the above-mentioned α-decay chain of $^{293}118$ to address the cause of failure in calculations of Smolańczuk [15], which guided the Berkeley retracted $Z = 118$ experiment. A similar α-decay chain is now observed [5] from the residual SHN $^{294}118$, after $3n$ emission from the CN $^{297}118^*$ formed in hot-fusion reaction $^{249}\mathrm{Cf} + ^{48}\mathrm{Ca}$. A first study of such α-decay chains from hot-fusion reactions is recently carried out by some of us [8] on the basis of extended PCM to include the excitation energy, equivalently temperature T, dependence. The T-dependent PCM, the PCM($T \neq 0$), is also applied to α-decay chain of $Z = 118$ SHN $^{294}118$, which is extended here in this paper to show that it removes the otherwise required scaling factor of 10^4 for α-decay half-lives calculated on PCM($T = 0$), applied to the above-noted cold-fusion reaction [14] and $^{287,288,289}115$ nuclei [16].

In addition to the above study, we have carried out an extensive calculation using PCM($T \neq 0$) to address the, not yet observed, but theoretically proposed [17,18], heavy cluster emissions from even-Z $^{294}118$, $^{290}116$, and $^{286}114$ parents occurring in α-decay chain of $^{294}118$. In our previous work [17,18] using PCM($T = 0$), we examined the possibility of heavy cluster decays of odd-Z $^{278}113$, $^{287-289}115$, and $^{293,294}117$ parents, corresponding to doubly magic $^{208}\mathrm{Pb}$ daughter or its neighboring nuclei. It is relevant to remind the reader here that PCM is the equivalent of using DCM for heavy-ion collisions at angular momentum $\ell = 0$, which finds its basis in quantum mechanical fragmentation theory (QMFT) [19]. Within this formulism, the cluster is assumed to be preformed in the parent (or mother) nucleus and the preformation probability for all possible clusters is calculated by solving the stationary Schrödinger equation for the dynamical flow of mass and charge. Note that the interaction potential (consisting of centrifugal term, the long-range Coulomb repulsive force and short-range nuclear attractive force) imparts the most critical input to investigate the decay (or formation) path of a nuclear system. Though the long-range Coulomb part of the potential is well known, the nuclear interaction part is as yet not fully understood and can be accounted for by using different proximity potentials. Therefore, in reference to the use of different proximity potentials, the α decay as well as heavy cluster emissions are analyzed first by using the PCM($T = 0$) and then by using PCM($T \neq 0$) with deformations included up to quadrupole (β_2) and hot "optimum" orientations [20] of nuclei. The calculations have been made by choosing nuclear proximity potentials Prox-1977 [21] and Prox-2000 [22] having different isospin and asymmetry dependence and then compared with other available theoretical calculations.

Finally, we have explored the significance of using $^{48}\mathrm{Ca}$ projectile for the synthesis of both odd- and even-Z SHEs. In other words, the structural aspects of the compound systems $^{285}113^*$, $^{292}114^*$, $^{291}115^*$, $^{296}116^*$, $^{297}117^*$, and $^{297}118^*$, formed in the reactions of $^{48}\mathrm{Ca}$ beam on $^{237}\mathrm{Np}$, $^{244}\mathrm{Pu}$, $^{243}\mathrm{Am}$, $^{248}\mathrm{Cm}$, $^{249}\mathrm{Bk}$, and $^{249}\mathrm{Cf}$ targets have been investigated at an excitation energy $E^*_{\mathrm{CN}} \sim 35$ MeV in terms of behavioral patterns of fragmentation potentials.

Summing up, the present work concerns the intensive experimental activity on the synthesis and study of $Z = 118$ SHE in recent years. The main aim of this paper is at least threefold, namely, (i) to study the decay cross sections of $2n$ and $3n$ ERs within the framework of DCM, with a view to see if the data observed refers to pure $^{249}\mathrm{Cf}$ isotope in the target and what would be the contribution of $^{250}\mathrm{Cf}$ if isotopic-mixed targets were used; (ii) to investigate the α-decay chain, and its possible competition with heavier cluster emissions from all the parents in the α-decay chain of $^{294}118$, for use of two different proximity potentials (Prox-1977 and Prox-2000) within the PCM approach at $T = 0$ and $T \neq 0$; and (iii) to make a comparative study of the structural aspects in $113 \leqslant Z \leqslant 118$ superheavy nuclei formed in $^{48}\mathrm{Ca}$-induced reactions.

The paper is organized as follows. Section II gives a brief description of the DCM and PCM with effects of deformations and orientation degrees of freedom included for coplanar configurations of nuclei [23]. The calculations and discussion of results are presented in Sec. III, and conclusions are summarized in Sec. IV. Brief reports of this work have been made at the National and International Conferences on Nuclear Physics [24,25].

II. THE DYNAMICAL CLUSTER-DECAY MODEL AND THE PREFORMED CLUSTER MODEL

The DCM for a hot and rotating CN is a reformulation of the PCM of Gupta and collaborators [26–28] for ground-state decays in exotic cluster radioactivity and related phenomenon. Following the QMFT, both models are worked out in terms of the coordinates of mass (and charge) asymmetry $\eta = (A_1 - A_2)/A$ [and $\eta_Z = (Z_1 - Z_2)/Z$], relative separation distance R, multipole deformations $\beta_{\lambda i}$ ($\lambda = 2, 3, 4$; $i = 1, 2$), and orientations θ_i of the two nuclei (1 and 2 stand, respectively, for heavy and light fragments). Using decoupled approximation to R and η motions, the DCM [16–20] defines the CN decay or fragments production cross section, in terms of ℓ partial waves, as

$$\sigma = \sum_{\ell=0}^{\ell_{\max}} \sigma_\ell = \frac{\pi}{k^2} \sum_{\ell=0}^{\ell_{\max}} (2\ell + 1) P_0 P, \quad k = \sqrt{\frac{2\mu E_{\mathrm{c.m.}}}{\hbar^2}}, \quad (1)$$

where, P_0, the preformation probability, refers to η motion and P, the penetrability, to R motion, both depending on ℓ, T, $\beta_{\lambda i}$, and θ_i. Here $\mu = mA_1A_2/(A_1 + A_2)$ is the reduced mass with m as the nucleon mass. $\ell_{\max}$ is the maximum angular momentum, defined later. Apparently, for $\ell = 0$,

$$\sigma_0 = \frac{\pi}{k^2} P_0 P, \quad (2)$$

which is an equivalent of the decay constant $\lambda = \nu_0 P_0 P$ or decay half-life $T_{1/2} = \frac{\ln 2}{\lambda}$ with ν_0 as the barrier assault frequency in PCM($T \neq 0$). In other words, for the $\ell = 0$ case, σ_0 and λ differ through a constant only. Thus, PCM($T \neq 0$) is equivalent to using DCM($\ell = 0$ case).

The preformation probability P_0 of the fragments in both PCM and DCM is obtained by solving the stationary

Schrödinger equation governing the η coordinate motion at a fixed $R = R_a$, defining the first turning point of the penetration path, taken same for different ℓ values,

$$\left[-\frac{\hbar^2}{2\sqrt{B_{\eta\eta}}}\frac{\partial}{\partial\eta}\frac{1}{\sqrt{B_{\eta\eta}}}\frac{\partial}{\partial\eta}+V_R(\eta,T)\right]\psi^{\nu}(\eta)=E^{\nu}_{\eta}\psi^{\nu}(\eta), \quad (3)$$

with $\nu = 0,1,2,\ldots$ referring to ground-state ($\nu = 0$) and excited-state solutions and the term $B_{\eta\eta}$ representing the smooth hydrodynamical masses [29]. The solution of this equation after normalization gives the preformation probability P_0 as

$$P_0 = |\psi[\eta(A_i)]|^2\frac{2}{A_{\rm CN}}\sqrt{B_{\eta\eta}}, \quad (4)$$

where P_0 contains the structural information of the CN which enters through the fragmentation potential $V_R(\eta,T)$, defined as

$$\begin{aligned}V_R(\eta,T) = &\sum_{i=1}^{2}[V_{\rm LDM}(A_i,Z_i,T)]+\sum_{i=1}^{2}[\delta U_i]\exp\left(-T^2/T_0^2\right)\\ &+V_C(R,Z_i,\beta_{\lambda i},\theta_i,T)+V_P(R,A_i,\beta_{\lambda i},\theta_i,T)\\ &+V_\ell(R,A_i,\beta_{\lambda i},\theta_i,T). \quad (5)\end{aligned}$$

Here $V_{\rm LDM}$ is the T-dependent liquid drop model energy of Davidson *et al.* [30] and δU is the "empirical" shell corrections from Myers and Swiatecki [31]. The other three terms V_C, V_P, and V_ℓ correspond to T-dependent Coulomb, nuclear proximity, and centrifugal potentials, respectively, whose details can be found, e.g., in Refs. [19,20]. The orientation angle θ_i is the angle between the nuclear symmetry axis and the collision Z axis, measured in the counterclockwise direction, and angle α_i is the angle between the symmetry axis and the radius vector $R_i(\alpha_i,T)$ of the colliding nucleus, measured in the clockwise direction from the symmetry axis. The deformations are taken up to quadrupole β_{2i} and the orientations are the "optimum" $\theta_i^{\rm opt}$ from Ref. [20]. The moment of inertia used here in V_ℓ is in the sticking limit, having the form $I_S(T) = \mu R^2 + \frac{2}{5}A_1 m R_1(\alpha_1,T)^2 + \frac{2}{5}A_2 m R_2(\alpha_2,T)^2$.

Whenever two nuclei approach each other within a very small distance, an additional attractive force will contribute to the total energy. The nuclear proximity potential for this additional attraction in Eq. (5) is defined as

$$V_P[s_0(T)] = 4\pi\bar{R}\gamma b(T)\Phi[s_0(T)], \quad (6)$$

where $b(T) = 0.99(1 + 0.009T^2)$ is the nuclear surface thickness, γ is the surface energy constant, and $\bar{R}(T)$ is the mean curvature radius (see Ref. [23] for more details). Φ is a universal function which is independent of the shapes of nuclei or the geometry of the nuclear system but depends on minimum separation distance $s_0(T)$. Two different versions of proximity potential, namely Prox-1977 and Prox-2000, having different isospin- and asymmetry-dependent parameters have been employed here in this work. The universal function for Prox-1977, given by Blocki *et al.* [21], is

$$\Phi(s_0) = \begin{cases}-\frac{1}{2}(s_0-2.54)^2-0.0852(s_0-2.54)^3,\\ -3.437\exp\left(-\frac{s_0}{0.75}\right),\end{cases} \quad (7)$$

respectively, for $s_0(T) \leqslant 1.2511$ and $s_0(T) \geqslant 1.2511$. However, for Prox-2000 version, Φ, taken from Myers and Swiatecki [22], is

$$\Phi(s_0) = \begin{cases}-0.1353+\sum_{n=0}^{5}[c_n/(n+1)](2.5-s_0)^{n+1}\\ \qquad\text{for}\quad 0 < s_0 \leqslant 2.5,\\ -0.095\,51\exp[(2.75-s_0)/0.7176]\\ \qquad\text{for}\quad s_0 \geqslant 2.5.\end{cases} \quad (8)$$

The values of different constants c_n are $c_0 = -0.1886$, $c_1 = -0.2628$, $c_2 = -0.152\,16$, $c_3 = -0.045\,62$, $c_4 = 0.069\,136$, and $c_5 = -0.011\,454$. For other features of these proximity potentials, refer to Refs. [21,22]. Because the two proximity potentials use different formulations, they give rise to barriers with different characteristics (height V_B, position R_B, and curvature $\hbar\omega$), and hence would result in different model parameters (for example, ΔR and $\ell_{\rm max}$ in DCM) for fitting of a given data. Some illustrative calculations for nuclei from heavy and superheavy mass regions are published [17,32,33] which, in general, support Prox-1977; rather it is another version, Prox-1988 (with a different surface energy constant γ) [34], not used here.

The barrier penetration probability P in Eq. (1) is given by the WKB integral

$$P = \exp\left(-\frac{2}{\hbar}\int_{R_a}^{R_b}\{2\mu[V(R)-Q_{\rm eff}]\}^{1/2}dR\right), \quad (9)$$

where R_b is the second turning point satisfying $V(R_a,T) = V(R_b,T) = Q_{\rm eff}$, with $Q_{\rm eff}$ as the effective Q value of the decay process. The first turning point R_a, taken to be the same for all ℓ values, is defined as

$$\begin{aligned}R_a &= R_1(\alpha_1,T)+R_2(\alpha_2,T)+\Delta R(T)\\ &= R_t(\alpha,T)+\Delta R(T), \quad (10)\end{aligned}$$

with the radius vectors

$$R_i(\alpha_i,T) = R_{0i}(T)\left[1+\sum_{\lambda}\beta_{\lambda i}Y_{\lambda}^{(0)}(\alpha_i)\right], \quad (11)$$

where T-dependent nuclear radii R_{0i}, taken from [35], are given by

$$R_{0i}(T) = \left[1.28A_i^{1/3}-0.76+0.8A_i^{-1/3}\right](1+0.0007T^2). \quad (12)$$

ΔR in Eq. (10), referred to as the neck-length parameter, is the separation distance between the surfaces of two fragments or clusters, which assimilates the deformation and neck formation effects between two nuclei, introduced within the extended model of Gupta and collaborators [27,36,37]. This method of introducing a neck-length parameter ΔR is similar to that used in both the scission-point [38] and the saddle-point [39] statistical fission models. The present calculations are found to be extremely sensitive to the choice of ΔR, which, in turn, decides the entry point of barrier penetration as well as of cluster's preformation probability. The choice of parameter R_a (equivalently, ΔR) for the best fit to the data corresponds to the effects of "barrier lowering" in it for each decay channel [refer to Fig. 1(a)], defined for each ℓ as the difference between $V_B(\ell)$ and $V(R_a,\ell)$, the barrier height and the actually used

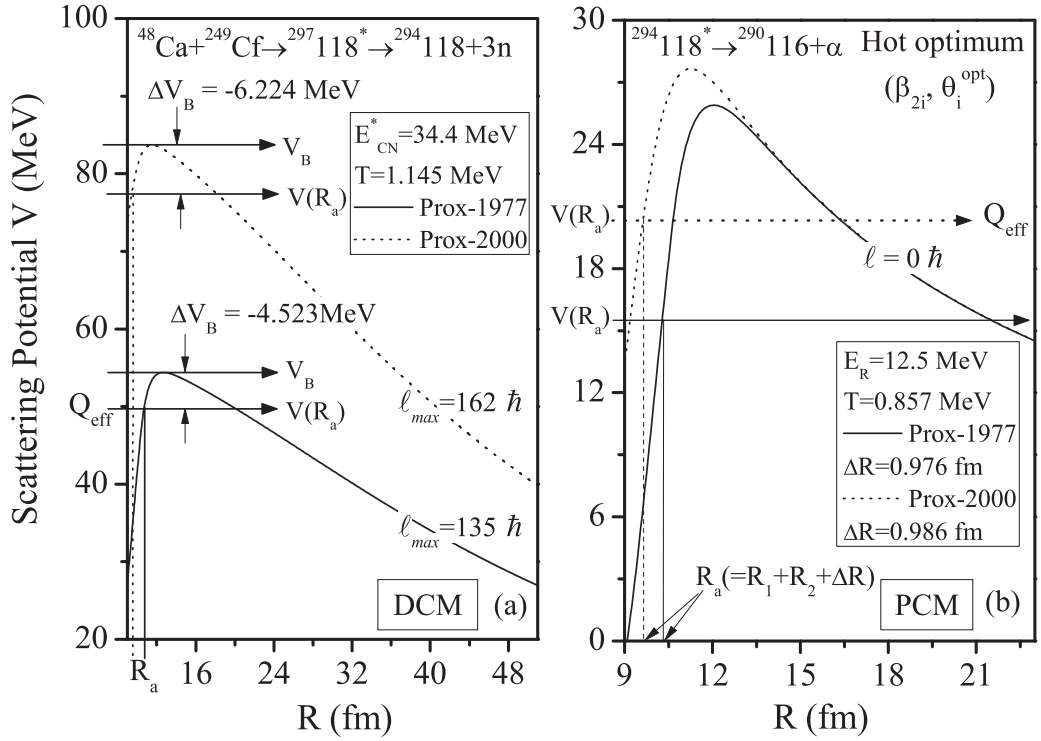

FIG. 1. (a) Scattering potentials $V(R)$ for $^{297}118^{*} \rightarrow {}^{294}118 + 3n$ using the DCM, at a fixed temperature $T = 1.145$ MeV, corresponding to $E^{*}_{\rm CN} = 34.4$ MeV, calculated at $\ell = \ell_{\rm max}$. The concept of barrier lowering $\Delta V_B = V(R_a) - V_B$ is also shown. (b) The same as for (a) but for α decay of $^{294}118^{*}$, formed in the ^{48}Ca + ^{249}Cf reaction after $3n$ emission, using the PCM at $T = 0.857$ MeV (equivalently, $E_R = 12.5$ MeV) for the $\ell = 0$ case. Solid lines are for the Prox-1977 and dotted lines are for Prox-2000 nuclear proximity potentials for deformed nuclei.

barrier, as

$$\Delta V_B = V(R_a, \ell) - V_B(\ell).$$

This is a built-in property of the DCM, illustrated in Fig. 1(a) for $3n$ decay of $^{297}118^{*}$ for the two proximity potentials. It may be worth noting that the use of the neck-length parameter, equivalently, "barrier modification," is the only acceptable explanation to date to account for the phenomenon of fusion hindrance at sub-barrier energies, because the effective barrier gets significantly modified [40,41].

The CN temperature T in DCM is given by $E_{\rm c.m.}$ and the Q value for incoming channel, as

$$E^{*}_{\rm CN} = E_{\rm c.m.} + Q_{\rm in} \tag{13}$$

shown in Fig. 1(a) for the illustrative case of $3n$ emission from $^{297}118^{*}$ nucleus. However, for the case of PCM($T \neq 0$), T is related to the recoil energy E_R of the (recoiled) residue SHN [8], whose excitation energy E^{*}_R for α decay is

$$E^{*}_R = E_R + Q_\alpha, \tag{14}$$

depicted in Fig. 1(b) for the $^{294}118^{*}$ nucleus, where both $E^{*}_{\rm CN}$ and E^{*}_R are related to T (in MeV) as

$$E^{*}_{\rm CN} = E^{*}_R = \tfrac{1}{11} A T^2 - T. \tag{15}$$

For the recoil energy E_R, we have taken the value of 12.5 MeV, which is chosen in reference to the average of the measured E_R range (7–18 MeV) [5] for the α-decay chain of the $^{294}118^{*}$ nucleus. The Q values are calculated by using binding energies from a 2003 experimental compilation of Audi *et al.* [42] and theoretical estimates of Möller *et al.* [43] whenever not available in Ref. [42]. Note that the concept of temperature in any quantum mechanical model, like the DCM or the PCM, is somewhat artificial, introduced through the statistical relation (15), and means simply the excitation energy in the system.

Finally, the assault frequency ν_0 in PCM($T \neq 0$) is given simply as

$$\nu_0 = \text{velocity}/R_0 = (2E_2/\mu)^{1/2}/R_0, \tag{16}$$

with total kinetic energy $E_1 + E_2 = Q_{\rm eff}$, with $E_2 = (A_1/A)Q_{\rm eff}$ for the case of decay from hot CN. This is illustrated in Fig. 1(b) for α decay of recoiled SHN.

III. CALCULATIONS AND DISCUSSION OF RESULTS

This section is divided into two parts. In Sec. III A, we present our calculations for the decay of CN $^{297}118^{*}$ formed in ^{249}Cf + ^{48}Ca reaction at $E_{\rm c.m.} = 204.53$ and 209.86 MeV (equivalently, at $T = 1.060$ and 1.145 MeV, respectively) using the DCM. The fragmentation potential $V(\eta)$, preformation probability P_0, penetrability P, their ℓ-summed values, xn ($x = 2$–4) evaporation channel cross sections, the decay barrier heights, and "barrier-lowering" effects are analyzed for related nuclear structure effects. Furthermore, we have calculated the cross sections for the residue nucleus $^{294}118^{*}$ synthesized in ^{250}Cf + ^{48}Ca reaction after the evaporation of four neutrons from $^{298}118^{*}$ CN. Finally, a comparative

TABLE I. DCM-calculated ER cross sections σ_{xn}, $x = 2$, 3, 4 for $^{297}118^{*}$ formed in the $^{48}\mathrm{Ca} + ^{249}\mathrm{Cf}$ reaction, at two different E^{*}_{CN}'s, compared with available experimental data for σ_{2n} and σ_{3n} [7], for β_2 deformed and optimum oriented nuclei. The neck-length parameter ΔR's given here in this table for $2n$-$4n$ emissions are for the best fit to data, and for light fragment masses $A_2 = 1$ and 5–148 (plus complementary heavy fragments), $\Delta R = 1$ fm for Prox-1977 nuclear potential at both the excitation energies. However, for Prox-2000, ΔR is taken to be 0.95 and 0.9 fm, respectively, for $E^{*}_{\mathrm{CN}} = 29.2$ MeV and $E^{*}_{\mathrm{CN}} = 34.4$ MeV for the $A_2 = 1$ fragment, whereas the same $\Delta R = 1$ fm is chosen for $A_2 = 5$–148 fragments at both energies.

E^{*}_{CN} (MeV)	T (MeV)	Decay channel	Prox-1977		Prox-2000		$\sigma^{\mathrm{expt.}}_{\mathrm{ER}}$ (pb)
			ΔR (fm)	$\sigma^{\mathrm{DCM}}_{\mathrm{ER}}$ (pb)	ΔR (fm)	$\sigma^{\mathrm{DCM}}_{\mathrm{ER}}$ (pb)	
29.2	1.060	$2n$	1.35	0.210	0.96	0.609	–
		$3n$	1.65	0.391	1.065	0.310	$0.3^{+1.0}_{-0.27}$
		$4n$	1.75	2.22×10^{-4}	1.2	1.80×10^{-2}	–
34.4	1.145	$2n$	1.35	0.837	0.92	0.825	$\leqslant 0.9$
		$3n$	1.628	0.597	1.02	0.468	$0.5^{+1.6}_{-0.30}$
		$4n$	1.75	7.50×10^{-4}	1.2	6.54×10^{-3}	–

analysis of the decay pattern of the various superheavy nuclei with $Z = 113$ to 118, formed in ^{48}Ca-induced reactions is explored. Then, in Sec. III B, the half-lives of α decays, along with the possibility of heavy cluster emission in the decay chain of recoiled SHN $^{294}118^{*}$, are studied within the framework of PCM($T \neq 0$). For comparisons, the α-decay half-lives are also calculated for the ground-state decays using PCM($T = 0$ case). All these calculations are performed by using two different versions of nuclear proximity potential, namely, Prox-1977 and Prox-2000, including the quadrupole deformations (β_{2i}) and "hot-optimum" orientations (θ_i) of decay fragments, taken from Table I of Ref. [20]. The "optimum" orientations are uniquely fixed on the basis of β_{2i} of nuclei alone. However, if one is interested in investigating the role of higher-order deformations, then "compact" orientations [44] should be used instead of optimum orientations. Also, it is important to remember here that, in reference to the earlier work [45,46] on the DCM, the magic numbers in the superheavy regions are taken as $Z = 126$ and $N = 184$.

A. Fusion-evaporation cross sections of $^{297}118^{*}$ and $^{298}118^{*}$ compound nuclei

First of all, we have tried to address the available data [7] for ER cross sections in reference to the decay of CN $^{297}118^{*}$ formed in the $^{249}\mathrm{Cf} + ^{48}\mathrm{Ca}$ reaction, by fitting the neck-length parameter (ΔR) of the DCM within the spherical fragmentation approach using Prox-1977. However, the measured cross sections [7] could not be achieved for any reasonable value of ΔR at both $E^{*}_{\mathrm{CN}} = 29.2$ and 34.4 MeV, which, in turn, suggests that the deformation effects may play an important role in the context of the present reaction. Consequently, we included the deformation effects of decay fragments up to quadrupole deformations (β_2), in reference to optimum orientations of hot compact configurations. Interestingly, the experimental data on neutron evaporation channels at both the excitation energies was adequately addressed for either of the two nuclear proximity potentials, Prox-1977 or Prox-2000. Besides, fortuitously, we found that the choice of Prox-2000 is also able to work reasonably well within the DCM for spherical fragments. Note that ΔR, defined in Eq. (10), is the only parameter of the model and controls the barrier lowering parameter ΔV_B described in Sec. II and depicted in Fig. 1(a).

Table I presents our DCM-calculated results for $2n$ and $3n$ decay cross sections σ_{2n} and σ_{3n} of CN $^{297}118^{*}$, using both nuclear potentials Prox-1977 and Prox-2000, with different neck-length parameters ΔR chosen to fit the respective experimental data [7] at the two E^{*}_{CN}'s. Also, σ_{4n} is given for comparison. Apparently, the DCM reproduces the experimental data nicely within one parameter fitting, indicating negligible contribution for $4n$ cross sections. The choice of different ΔR's for different decay channels (here xn) justifies their occurrence in different time scales.

We have also made a calculation, similar to one above, for $4n$ decay cross section of $^{298}118^{*}$, formed in the $^{250}\mathrm{Cf} + ^{48}\mathrm{Ca}$ reaction, using the nuclear potentials Prox-1977 and Prox-2000, at the two above-mentioned E^{*}_{CN}'s, taking the same ΔR as obtained in Table I for $^{297}118^{*}$. We get $\sigma_{4n} = 1.31 \times 10^{-3}$ pb and 3.54×10^{-3} pb for Prox-1977 and 6.43×10^{-2} pb and 5.93×10^{-2} pb for Prox-2000, respectively, at $E^{*}_{\mathrm{CN}} = 29.2$ and 34.4 MeV. Interestingly, these DCM-calculated cross sections are of orders similar to those obtained on the DCM in Table I for σ_{4n} of CN $^{297}118^{*}$ formed in the $^{249}\mathrm{Cf} + ^{48}\mathrm{Ca}$ reaction. Apparently, measurements of such data would be of interest, particularly for isotope-mixed targets.

To see the relative contributions of Prox-1977 and Prox-2000 potentials, we have plotted in Fig. 2 the barrier height V_B as a function of angular momentum ℓ varying from ℓ_{min} to ℓ_{max}, fixed later in Fig. 4 (refer to Fig. 1 for the barriers in the two cases). It is evident that, independent of the choice of proximity potential, V_B increases with increase of ℓ. A higher barrier height V_B is obtained for Prox-2000, as compared to that for Prox-1977, and the difference is a little more at higher ℓ values. Note that the angular momentum ℓ values involved are too high and hence the barriers are too high (ℓ windows for Prox-1977 and Prox-2000 are $69 \leqslant \ell \leqslant 135$ and $86 \leqslant \ell \leqslant 162$, respectively). The barriers for $\ell < \ell_{\mathrm{min}}$ values are not shown because they do not contribute to the relevant decay cross section. The variation of barrier modification ΔV_B with ℓ is also shown as an inset of the figure. It is relevant to

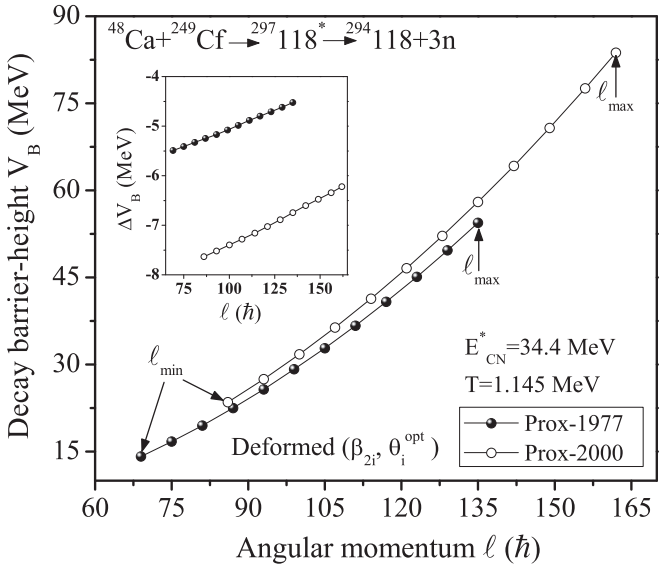

FIG. 2. Variation of the barrier height V_B as a function of angular momentum ℓ varying from ℓ_{min} to ℓ_{max} ($\ell < \ell_{min}$ values do not contribute; see text) for the $3n$ decay of the $^{297}118^*$ CN at $E^*_{CN} = 34.4$ MeV, with use of Prox-1977 and Prox-2000. The comparison of "barrier-lowering" parameter ΔV_B is also shown as an inset.

recall here again that barrier lowering is a built-in property of the DCM which has direct dependance on the value of neck-length parameter ΔR. One may observe that, for the $3n$ decay channel at $E^*_{CN} = 34.4$ MeV, ΔV_B turns out to be small for Prox-1977, as compared to that for Prox-2000. Apparently, ΔV_B decreases in magnitude with the increase in ℓ, and one may conclude that much barrier modification is needed for lower angular momentum values.

To investigate further the importance of deformation effects, Fig. 3 shows the fragmentation potential $V(A_2)$,

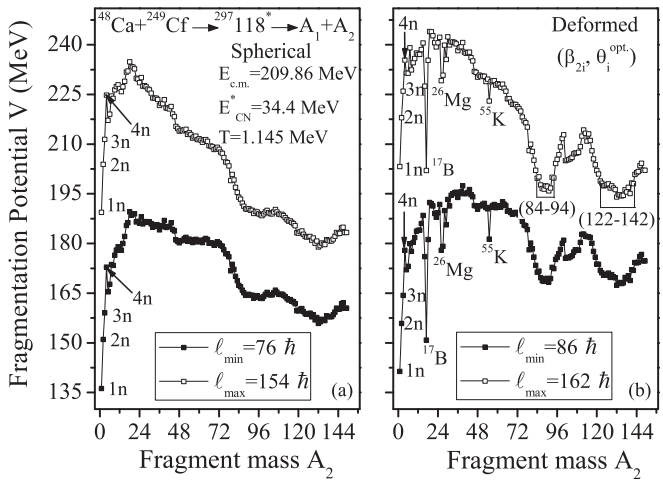

FIG. 3. Mass fragmentation potential for $^{297}118^*$ using Prox-2000 potential for (a) spherical and (b) deformed configurations. For spherical nuclei, the ΔR values for the best fit to data are 1.0, 1.17, 1.28, 1.3, and 1.0 fm, respectively, for light fragment masses $A_2 = 1$, 2, 3, 4, and 5–148 at $E^*_{CN} = 34.4$ MeV for the ^{48}Ca + ^{249}Cf reaction. The same for the deformed case are given in Table I.

minimized in charge coordinate η_Z, plotted for the case of Prox-2000 at the two extreme ℓ values for both the spherical as well as deformed considerations. The deformations $\beta_{\lambda i}$ for $\lambda = 2$, $i = 1$, 2, have been taken from Ref. [43], given for $Z \geqslant 8$, $A \geqslant 16$. However, for $Z < 8$, deformations β_{2i} are from relativistic mean-field calculations [47] because the same is not known experimentally for all decay products entering the calculations. As noted above at the beginning of Sec. III A, though unexpected owing to smoothed potential energy surfaces [Fig. 3(a)], the measured values of σ_{2n} and σ_{3n} are attained for a spherical choice of fragments using the best-fit ΔR values (given in caption of Fig. 3) at $T =$ 1.145 MeV, corresponding to one of the excitation energy $E^*_{CN} = 34.4$ MeV, for use of Prox-2000 only. We notice in Fig. 3 that the contribution of fusion ERs (LPs: $1n$, $2n$, $3n$, and $4n$) is prominent (lower in energy) at $\ell = \ell_{min}$, whereas fission fragments start dominating in the decay process at $\ell = \ell_{max}$. Interestingly, with the inclusion of deformation and orientation effects, one can clearly see strong variations in the structure of potential energy surfaces [Fig. 3(b)] which otherwise remains smooth for spherical choice of fragments [Fig. 3(a)]. As a result, the relative preformation probability P_0 for all fragments gets modified accordingly. Some extra valleys at ^{17}B, ^{26}Mg, and ^{55}K nuclei are observed in the case of deformed configurations, which arise possibly owing to the inappropriate β_{2i} values used here [43,47]. However, these deeper minima do not affect the total cross section as they get ruled out owing to very small penetrability P across the appropriate interaction barrier, as shown later in Fig. 5. Also, the fragmentation potential in Fig. 3(b) favor two strong minima at $A_2 = 84$–94 and $A_2 = 122$–142, which refer to the not-yet-observed FF channel in the decay of $^{297}118^*$ for the deformed case. An experimental verification of these predictions would be of further interest. From this discussion, we may conclude that the indispensable role of deformations and orientations is essential for understanding the neutron evaporation process in the decay of superheavy compound systems.

Knowing that the CN decay cross section in DCM is a combined effect of both the preformation probability P_0 and the penetrability P, Figs. 4(a) and 4(b) show the variations of calculated P_0 and P for $2n$ and $3n$ decay channels (or clusters emitted) from $^{297}118^*$ as a function of angular momentum ℓ for both Prox-1977 and Prox-2000 potentials. Interestingly, these figures fix the ℓ_{max} and ℓ_{min} values, respectively, beyond which the contributions to cross sections become negligible. In other words, they fix the limited range of angular momentum between ℓ_{min} and ℓ_{max} values, which give significant contribution to the total cross section. One can clearly see that both xn ($x = 2$, 3) clusters are favorably preformed for ℓ values right from zero to about 110$\hbar$ and 130$\hbar$, respectively, for Prox-1977 and Prox-2000, but then P_0 falls off nearly suddenly. Using the definition of ℓ_{max} as the one where P_0 of light particles tends to zero, and setting the limiting value of $P_0 < 10^{-14}$, we can set from Fig. 4(a) $\ell_{max} = 135\hbar$ and 162$\hbar$, respectively, for Prox-1977 and Prox-2000 nuclear potentials, though the value of ℓ at which the preformation process nearly stops is slightly different for different neutron emissions. However, in contrast to P_0, Fig. 4(b) depicts that the

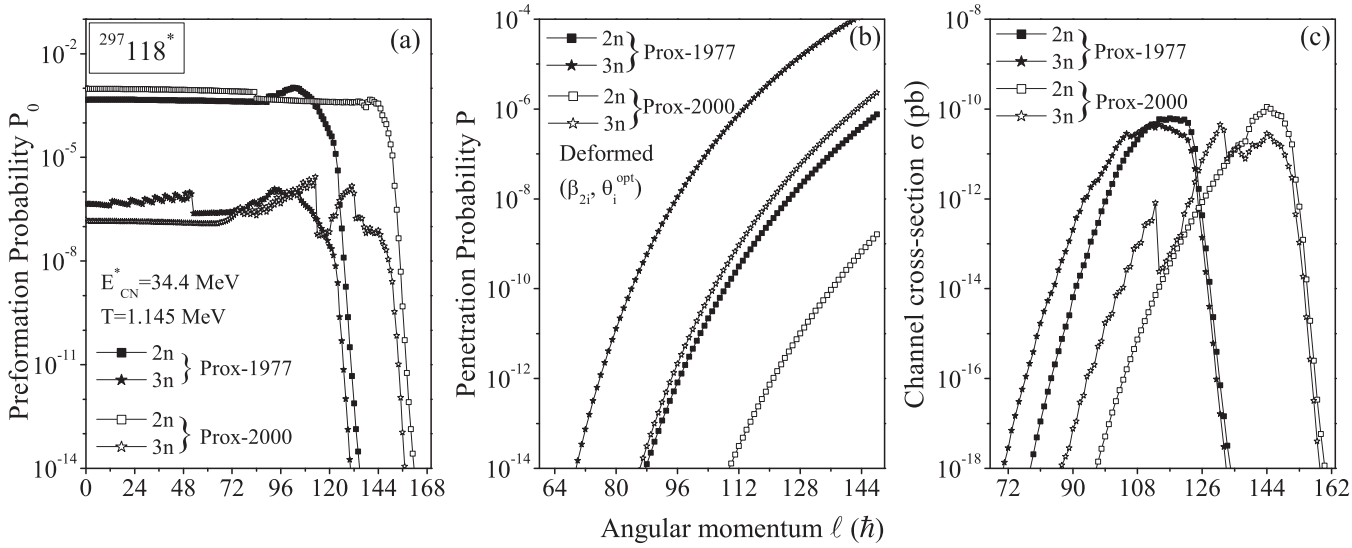

FIG. 4. (a) Preformation probability P_0, (b) WKB penetration probability P, and (c) the channel cross sections σ_{2n} and σ_{3n} as functions of ℓ for the two proximity potentials, illustrated for $E^{*}_{CN} = 34.4$ MeV, for CN $^{297}118^{*}$ with deformations up to β_2 and optimum orientations.

contribution of P goes on increasing as the ℓ value increases, irrespective of the choice of different proximity potentials. In other words, while the preformation factor P_0 for $2n$ and $3n$ clusters decreases, the penetrability P increases as one goes from lower to higher ℓ values. By fixing the lower limit of $\ell = \ell_{\min}$ for the contributions of $P < 10^{-14}$ not included, we have here in Fig. 4(c) an upper ($\ell_{\max}$) as well as lower ($\ell_{\min}$) limits on ℓ values that contribute towards the channel cross sections σ_{xn} for $x = 2, 3$. It is to be noted that the channel cross section follows the same trend for both the potentials and the ℓ window corresponds to $69\hbar$–$135\hbar$ for the Prox-1977 potential and that for Prox-2000 it is approximately $86\hbar$–$162\hbar$. The difference between the two cases lies in the fact that higher value of $\ell_{\max}$ and corresponding lower value of ΔR (see Table I) is required to fit the available $2n$ and $3n$ channel cross sections with the use of Prox-2000 as compared to Prox-1977. This happens because the barriers for the two proximity potentials come out to be different (see Fig. 1) and hence consequently a smaller neck length is required for the use of Prox-2000, in comparison to Prox-1977. Apparently, we notice from Fig. 4 that both P_0 and P depend significantly on the type of nuclear interaction potential used, thereby affecting the CN decay cross section.

Figure 5 shows the ℓ-summed preformation probability P_0, penetrability P, and cross section σ, with summation up to $\ell = \ell_{\max}$, as a function of fragment mass number for the two proximity potentials. It can be seen from this figure that σ follows the trend of P_0, which shows an interesting structure with significant preformation factors for both the heavy mass fragments (HMFs) and asymmetric fission fragments (AFFs). The fragments in the mass range $A_2 = 84$–94 and $A_2 = 122$–142 (plus their complementary heavy fragments also), corresponding to HMFs and AFF peaks seem to contribute toward fission cross sections, though no such fragments are identified in the experiment [7]. Also, we notice that summed P is almost constant and thus contributes mainly to the magnitude of the cross section. The strongly preformed fragments ^{17}B, ^{26}Mg, and ^{55}K in Fig. 5, which also occur as strong minimum in the fragmentation potential of Fig. 3(b), are shown to have very small penetrability. Hence, these do not have any significant contribution towards final cross section. Comparing Prox-1977 with Prox-2000, we find significant changes in the fission valley structure of the preformation yield and, as a result these differences, could provide some new insight into the understanding of nuclear structure effects related to the decay of $^{297}118^{*}$ nucleus.

Next we have investigated the significance of using ^{48}Ca as a projectile for the synthesis of SHEs within the dynamical fragmentation theory. Specifically, we have considered the compound systems $^{285}113^{*}$, $^{292}114^{*}$, $^{291}115^{*}$, $^{296}116^{*}$, $^{297}117^{*}$, and $^{297}118^{*}$ formed in the reactions of ^{48}Ca beam on ^{237}Np, ^{244}Pu, ^{243}Am, ^{248}Cm, ^{249}Bk, and ^{249}Cf targets.

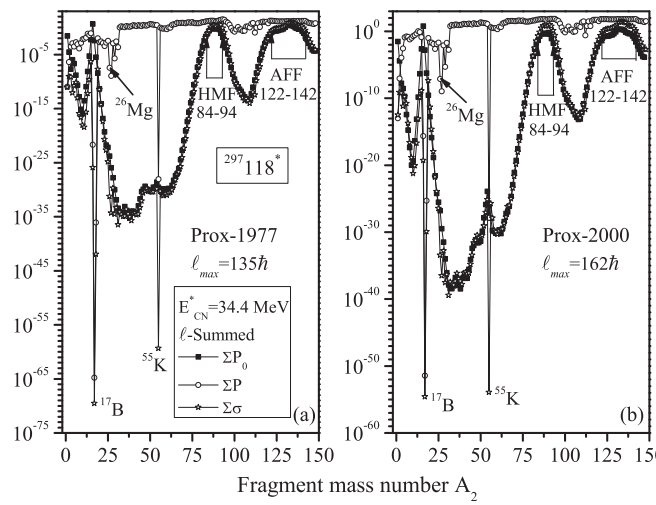

FIG. 5. Decay cross section σ, penetration probability P, and preformation probability P_0, summed over ℓ, plotted as a function of light fragment mass number A_2 for the compound system $^{297}118^{*}$ formed in the $^{48}\text{Ca} + ^{249}\text{Cf}$ reaction, for (a) Prox-1977 and (b) Prox-2000.

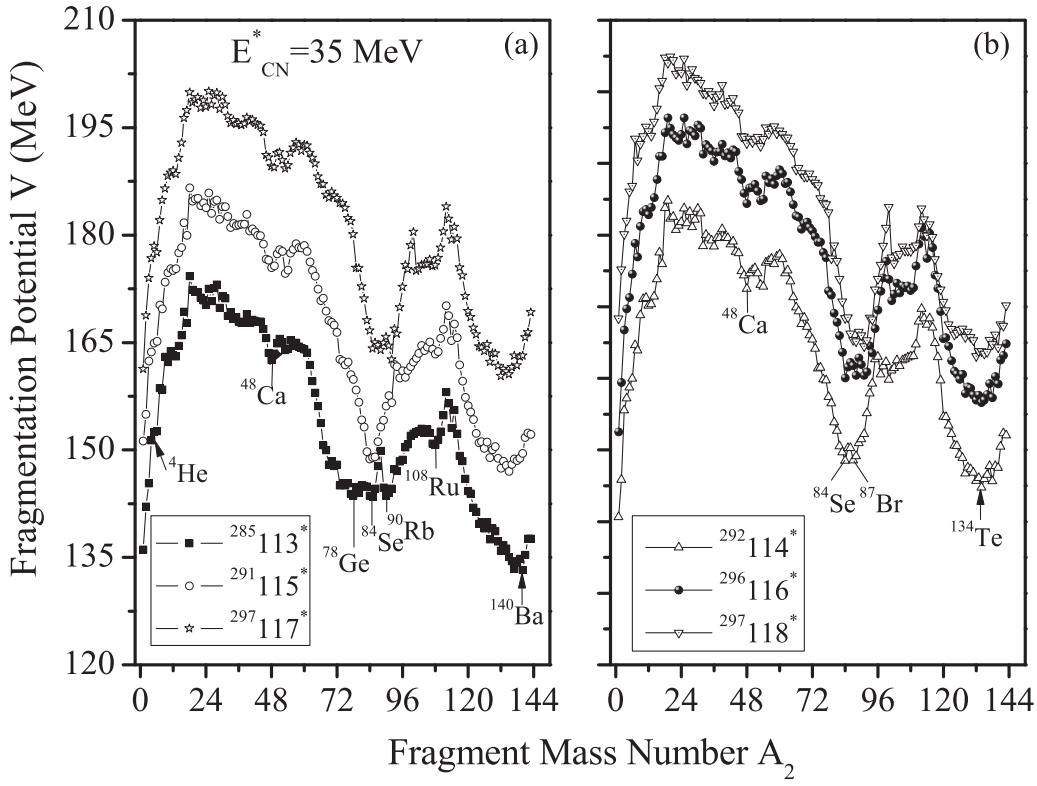

FIG. 6. Mass fragmentation potentials $V(A_2)$ for various excited compound systems with $Z = 113$–118 corresponding to $E^*_{CN} = 35$ MeV, having β_{2i} deformations and optimum orientations included, for the case of Prox-1977. $\Delta R = 1.5$ fm with the corresponding $\ell \approx 100\hbar$, chosen arbitrarily, and are kept the same in all cases for comparisons.

Figures 6(a) and 6(b) show the calculated fragmentation potentials, based on Eq. (5), respectively, for the formation or decay of odd- and even-Z systems [48], with deformations up to β_2 and for the case of Prox-1977 only. The calculations are made for an excitation energy $E^*_{CN} \sim 35$ MeV to study the comparative behavior of the formation or decay mechanism. Note that the above-mentioned systems are formed at a fixed ΔR, in contrast to the fragmentation profile in Fig. 3, where different decay products are considered to occur in different time scales and hence different ΔR's were used. We notice in Fig. 6 that, in each case, there is a minimum corresponding to the ^{48}Ca nucleus in addition to at least two other minima referring to heavy mass and asymmetric mass fragments, which, in turn, allows us to make significant observations about the structural aspects in $113 \leqslant Z \leqslant 118$ superheavy nuclei, as well as their decay products. The fission valleys near $A_2 = 82$–92 and 132–142 are reinforced owing to a deformed magic shell around $Z_2 = 36$ and spherical magic shell around $Z_2 = 50$.

B. α-decay chain of SHN ^{294}118* and its possible competition with heavier cluster emissions from all parents in the α-decay chain

As stated in the Introduction, most of the SHNs decay primarily through consecutive α-emissions and end up with known α- or spontaneous-fissioning nucleus. Figure 1 in Ref. [8] illustrates schematically the possible decay modes of a CN with excitation energy E^* via the α-decay chain and the CN fusion process. Therefore, an attempt is made in this section to analyze the α-decay half-lives $T^{\alpha}_{1/2}$ within the framework of PCM with $T = 0$ and $T \neq 0$, for the measured decay chain of ^{294}118* formed via ^{249}Cf + ^{48}Ca $\rightarrow$ ^{297}118* reaction after the $3n$ emission [5]. In addition, we have calculated the possible branching of α decay to the most probable cluster decays, with an idea to investigate the role of spherical and deformed magic shell closures of the daughter nucleus in the process of exotic cluster emission.

In view of our earlier work [16] on PCM($T = 0$), applied to the decay of ^{287,288,289}115 superheavy nuclei, we first analyzed the α-decay chain of ^{294}118 using Prox-1977 within PCM($T = 0$) for spontaneous decays, including quadrupole deformations β_{2i} and optimum orientations θ_i, taking the view that decay fragments get settled in the ground state. As expected, we find that the PCM($T = 0$)-calculated half-lives for the measured [5] decay chain of ^{294}118 agree with experimental data with in a constant empirical factor of 10^4, for the value of neck length ΔR lying in the range of 1.0–1.7 fm (see Table II, last column). However, the experimental data could not be addressed to for the use of the Prox-2000 potential. Therefore, one may conclude that, for spontaneous α decays of superheavy nuclei, the use of Prox-1977 is relatively better than Prox-2000.

As a next step, following our recent study [8] based on Prox-1977, we have investigated the possibility of including temperature T effects in PCM, i.e., use PCM($T \neq 0$) to

TABLE II. Comparison of experimental α-decay half-lives for $Z = 114$–118 SHEs occurring in α-decay chain of $^{294}118$, synthesized in $^{48}Ca + ^{249}Cf$ reaction via $3n$ emission, with our PCM($T \neq 0$) calculations, using different nuclear proximity potentials (Prox-1977 and Prox-2000) at a temperature equivalent of recoil energy $E_R = 12.5$ MeV and other available theoretical results. Calculated half-lives using PCM($T = 0$) for Prox-1977 for the deformed choice of nuclei are also listed.

α decay of	ΔR (fm)		Half-lives, $T^{\alpha}_{1/2}$ (ms)							
	PCM ($T \neq 0$)				Expt. [5]	CYEM [49]	CPPMDN [50]	DDM3Y [51]	GLDM [52]	PCM($T = 0$) $\times 10^4$
	Prox-1977	Prox-2000	Prox-1977	Prox-2000						Prox 1977
$^{294}118$	0.976	0.986	0.69	0.65	$0.69^{+0.64}_{-0.22}$	2.188	$0.53^{-0.16}_{+0.22}$	$0.66^{+0.23}_{-0.18}$	$0.15^{+0.05}_{-0.04}$	0.69
$^{290}116$	0.950	0.938	8.51	8.57	$8.3^{+3.5}_{-1.9}$	56	$20.8^{-8.2}_{+13.8}$	$13.4^{+7.7}_{-5.2}$	$3.47^{+1.99}_{-1.26}$	8.39
$^{286}114$	0.941	0.934	118	118	120^{+40}_{-20}	831.7	170^{-60}_{+90}	160^{+70}_{-50}	50^{+20}_{-20}	119

account for the fact that the (residual) superheavy nucleus $^{294}118^{*}$, left after $3n$ emission, has a recoil energy E_R (=7 to 18 MeV from experiments [5]) associated with it. Table II shows the results of our calculated α-decay half-lives $T^{\alpha}_{1/2}$ and other characteristic quantities (the neck-length ΔR's) for use of Prox-1977 and Prox-2000 potentials at an average (fixed) $E_R = 12.5$ MeV to superheavy nuclei $Z = 118$, 116, and 114 occurring in α-decay chains of $^{294}118^{*}$. Table II also shows a comparison of our PCM($T \neq 0$) for the two proximity potentials with other available theoretical formalisms such as cubic plus yukawa plus exponential (CYE) model [49], the Coulomb and proximity potential model for deformed nuclei (CPPMDN) [50], the density-dependent M3Y (DDM3Y) effective interaction [51], and the generalized liquid drop model (GLDM) [52]. Interestingly, in agreement with our earlier result [8], Table II shows that our PCM($T \neq 0$) calculations agree nicely with the experimental data without any multiplying factor and that this result is independent of the choice of proximity interaction. Another interesting result to note in Table II is that the α-decay half-life for $^{286}114$ is higher than for $^{290}116$ and $^{294}118$ parents, which means that the $Z = 114$ parent nucleus is more stable against α emission than the $Z = 116$ and 118. The stability of $^{286}114$ can be attributed to the expected magicity of protons at $Z = 114$, or of neutrons at $N = 172$, or both.

Furthermore, the competition of α decay with other possible heavier-cluster emissions is also probed by investigating the potential energy surfaces (PESs) in terms of preformation factors P_0, presented in Fig. 7 for the whole decay process of $^{294}118^{*}$ at the temperature equivalent of recoil energy $E_R = 12.5$ MeV. Precisely, P_0 measures the probability with which the cluster or fragment is preformed inside the CN, before it penetrates the interaction barrier. Note that P_0 follows a relative distribution, which means that a slight change in the fragmentation potential at any fragment leads to a redistribution of P_0 among all the fragments. We find that, in addition to the α particle, the most prominent clusters are ^{48}Ca and a heavier cluster, like ^{80}Ge, ^{84}Se, and ^{86}Kr, emitted from $Z = 114$, 116, and 118 parent, respectively. This result is found independent of changing the nuclear proximity potential, despite the fact that the PESs are slightly modified. Note that ^{48}Ca is a doubly magic nucleus, and the daughter nucleus of heavy clusters is the doubly magic ^{208}Pb or its neighboring nucleus, in agreement with our recent work [17] on PCM($T = 0$).

Figure 8 presents the PCM($T \neq 0$)-calculated preformation P_0 and penetration P probabilities for α- and other most-probable cluster decays from each of the parents in the α-decay chain of the $^{294}118^{*}$ nucleus. One can clearly see that ^{4}He is always preformed with the largest probability (smallest $-\log_{10}P_0$ value), though its P values are very small. The nuclear shell structure effects are also clearly visible in P_0 by its being larger for clusters referring to doubly closed shell ^{208}Pb or its neighboring daughter nucleus. We further notice that heavy clusters ^{86}Kr, ^{84}Se, and ^{80}Ge are preformed with larger P_0 values, compared to ^{48}Ca, respectively, in $^{294}118^{*}$, $^{290}116^{*}$,

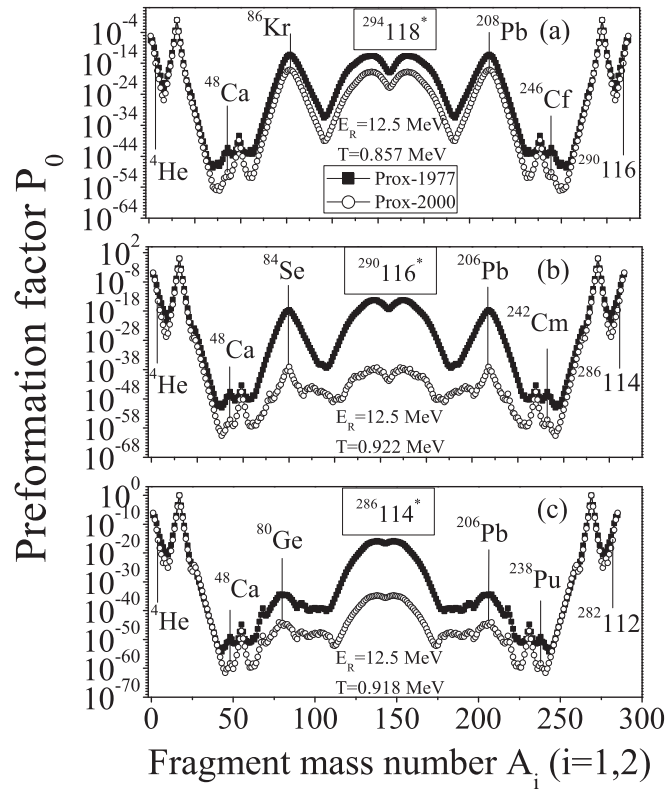

FIG. 7. Preformation probability P_0 for the decay of all the parents occurring in α-decay chain of $^{294}118^{*}$ using PCM($T \neq 0$) for nuclear potentials Prox-1977 and Prox-2000 at recoil energy $E_R = 12.5$ MeV. Calculations are done using β_{2i} deformations and "hot" optimum orientations for all the possible combinations at the respective ΔR values given in Table II.

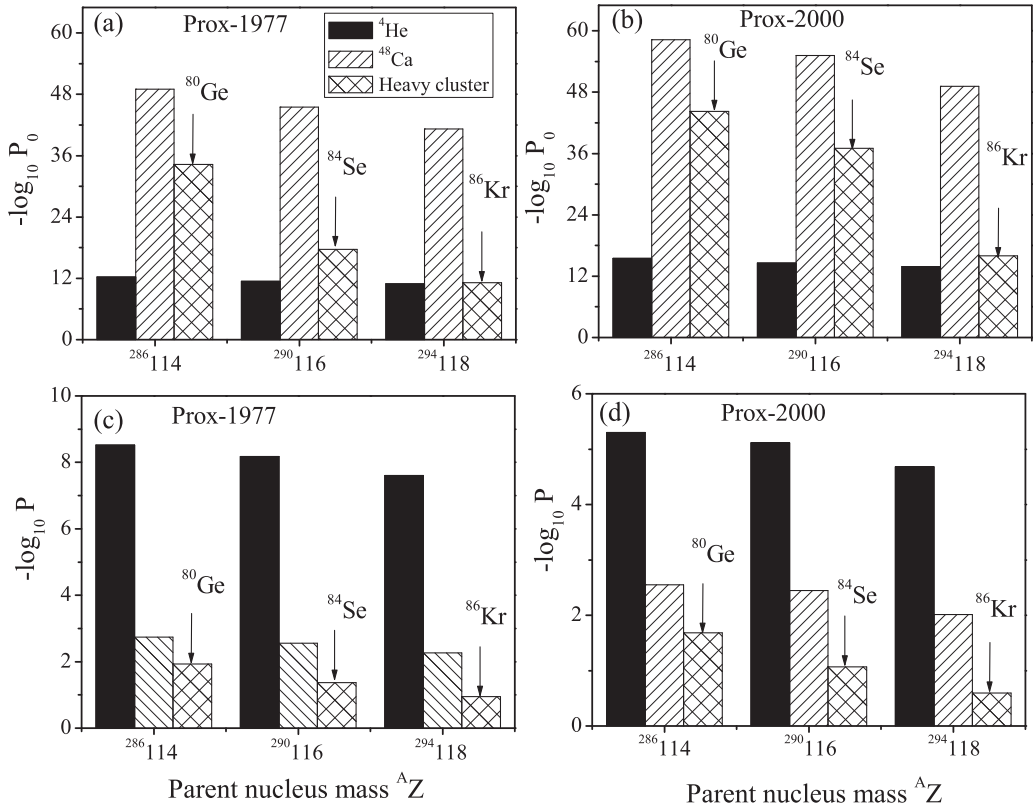

FIG. 8. (a),(b) Preformation and (c),(d) penetration probability for α and most-probable cluster decays of the parents occurring in α-decay chain of $^{294}118^{*}$, using nuclear potentials Prox-1977 and Prox-2000 for deformed (up to β_2) choice of fragments.

and $^{286}114^{*}$ parents. This happens because the deformed shell effects at $Z_2 = 36$ for light fragments or heavy clusters (actually at $Z_2 = 36$, 34, and 32) reinforces the spherical shell closure at $Z_1 = 82$ (^{208}Pb) for a heavy fragment. This result holds well despite the use of different nuclear proximity potentials, thereby providing important information for the overall understanding of cluster dynamics from a variety of parent nuclei.

The consequences of the above results, for P_0 and P, are shown explicitly for the half-life time $T_{1/2}$ in Fig. 9 for both choices of the nuclear proximity force. We notice that our calculated $T^{\alpha}_{1/2}$ agrees nicely with the experimental data, which, in turn, gives a confidence that our model may impart a reasonable estimate of the most probable emitted heavier clusters. Because $T_{1/2}$ is a combined effect of both P_0 and P (ν_0 being a constant, $\sim 10^{21}$ s^{-1}), we observe in Fig. 9 that, in addition to the α decay, the clusters corresponding to doubly magic ^{208}Pb, or its neighboring daughter nucleus, have minimal decay half-lives, independent of the choice of nuclear proximity potential. As noted above, this effect is solely attributable to the combined effect of spherical doubly magic ^{208}Pb and the deformed magic shells around $Z_2 = 36$. However, for the ^{48}Ca cluster, though doubly spherical magic, the predicted decay half-life lies far above the heavy clusters (even above the present limit $\log_{10} T_{1/2} \leqslant 29$ s of experimental methods) because of the heavier fragment (^{246}Cf, ^{242}Cm, or ^{238}Pu) being a strongly deformed nucleus. Thus, the present study indicates the interesting possibility of heavier clusters like ^{86}Kr, ^{84}Se, and ^{80}Ge, in addition to α decay, for the decay of $^{294}118^{*}$ and its subsequent parents ending the chain in $^{286}114^{*}$.

Finally, we notice that the above predictions are made purely on the basis of best-fit ΔR values obtained in reference to the measured α-decay half-lives in the decay

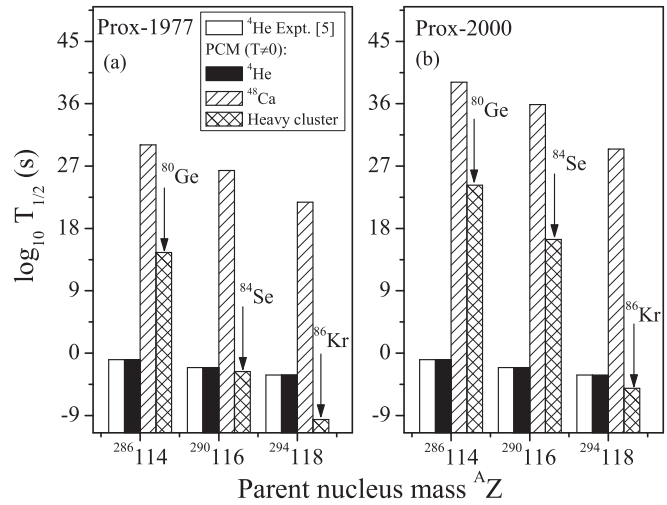

FIG. 9. The logarithm of decay half-lives calculated on PCM($T \neq 0$) for α and other cluster decays using (a) Prox-1977 and (b) Prox-2000 potentials, plotted as a function of parent nucleus mass for the α-decay chain of $^{294}118^{*}$.

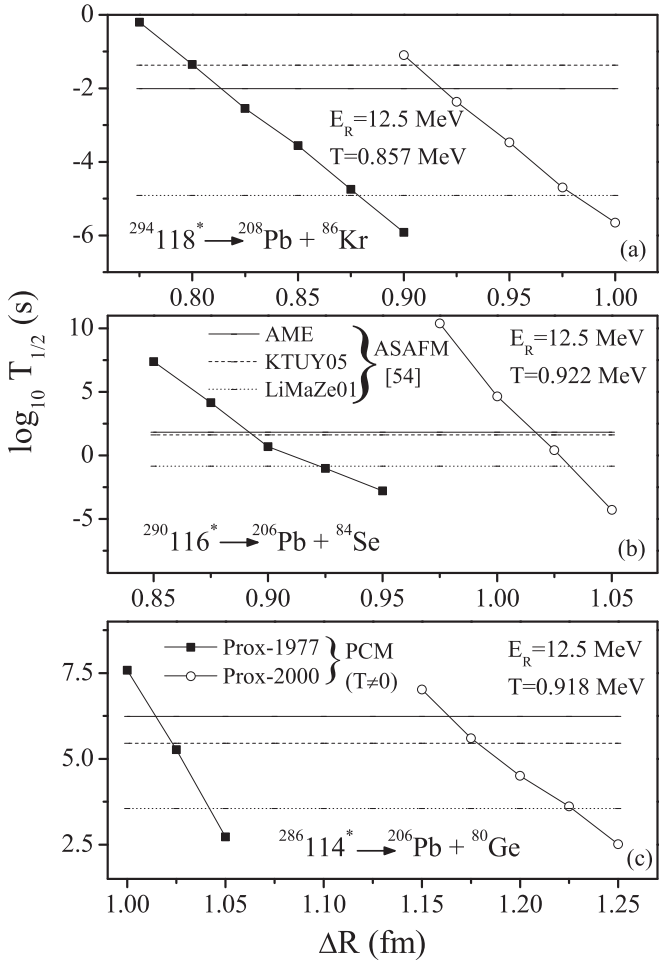

FIG. 10. Predicted decay half-life times using PCM($T \neq 0$) over a wide range of neck-length values for the most favored heavy clusters emitted from (a)$^{294}118^{*}$, (b) $^{290}116^{*}$, and (c) $^{286}114^{*}$ parents resulting in a doubly magic ^{208}Pb or its neighboring daughter nucleus, compared with the predictions of ASAFM for different mass tables.

chain of $^{294}118^{*}$ for use of PCM($T \neq 0$) at $E_R = 12.5$ MeV (refer Table II). Because the choice of ΔR is extremely sensitive in PCM calculations, we have made an effort in Fig. 10 to predict decay half-lives over a range of ΔR for the most-probable heavy clusters emitted from $^{294}118^{*}$, $^{290}116^{*}$, and $^{286}114^{*}$ parents with decay products treated as deformed and oriented nuclei. Note that this study is an extension of our very recent work [17,18] carried out using PCM($T = 0$) for the ground-state cluster decays of $^{278}113$, $^{287–289}115$, and $^{293,294}117$ parents. In the present work, however, the half-lives have been calculated using PCM($T \neq 0$) and then compared with the predictions of analytic superasymmetric fission model (ASAFM) [53,54]. Figure 10 shows this comparison of our PCM($T \neq 0$)-calculated half-lives with the predictions of ASAFM, obtained by using different mass tables AME11 (Atomic Mass Evaluation), LiMaZe01 (Liran-Marinov-Zeldes), and KTUY05 (Koura-Tachibana-Uno-Yamada). As expected, $\log_{10}T_{1/2}$ values for the three clusters, respectively, from $^{294}118^{*}$, $^{290}116^{*}$, and $^{286}114^{*}$ parents are significantly influenced by the variation of ΔR, thereby giving different contributions for both choices of nuclear potentials. However, at present this study of heavy cluster decays is more of a theoretical interest from the point of view of its possible measurements.

IV. SUMMARY AND CONCLUSIONS

Summarizing, we have investigated the role of different proximity interactions for the decay of $^{297,298}118^{*}$ superheavy compound systems formed in the $^{249,250}\mathrm{Cf} + {}^{48}\mathrm{Ca}$ reactions, using the DCM. By including the quadrupole (β_{2i}) deformations, together with the optimum orientations, the DCM calculated $2n$ and $3n$ ER cross sections, using both Prox-1977 and Prox-2000, find a nice comparison with experimental data for the $^{249}\mathrm{Cf} + {}^{48}\mathrm{Ca}$ reaction at two incident energies. However, the relative contribution of σ_{4n} in the $^{250}\mathrm{Cf} + {}^{48}\mathrm{Ca}$ reaction, though of the same order as $4n$ channel in the $^{249}\mathrm{Cf} + {}^{48}\mathrm{Ca}$ reaction, comes out to be much smaller in comparison to its observed $3n$ channel. Apparently, further experiments are needed for the verification of $4n$ component in the reactions under study.

A possible contribution from the, not yet observed, FF component, constituted of both heavy mass and asymmetric mass fragments, is also indicated. Other important results are as follows. (i) The barrier height is shown to get strongly modified with the use of different nuclear potentials. (ii) The barrier-lowering parameter ΔV_B is found to be lower for Prox-1977. (iii) A relatively smaller value of neck parameter is required for the use of Prox-2000, as compared to the Prox-1977 potential. In addition, a comprehensive study of the structural aspects is worked out for $113 \leqslant Z \leqslant 118$ superheavy nuclei formed in ^{48}Ca-induced reactions.

Finally, the results of α-decay half-lives of $^{294}118$, and its subsequent $^{290}116$ and $^{286}114$ parents occurring in the decay chain, are presented within the formalism of PCM, which, in turn, provides a unique opportunity to comment on the conclusive role of temperature T dependence in its built-in preformation and penetration probabilities of decay fragments. The competition of α decay with other possible heavy cluster emissions from all the parents in the α-decay chain is also probed with a view to understand further the nuclear structure effects involved, though to date these are more of theoretical interests than their possible observation.

ACKNOWLEDGMENTS

Work supported by the University Grants Commission (UGC), New Delhi, India, under Grant No. F.13-901/2013(BSR) of Dr. D. S. Kothari Program.

[1] S. Hofmann and G. Münzenberg, Rev. Mod. Phys. **72**, 733 (2000).
[2] S. Hofmann, Radiochim. Acta **99**, 405 (2011).
[3] K. Morita *et al.*, J. Phys. Soc. Jpn. **76**, 045001 (2007).
[4] Yu. Ts. Oganessian *et al.*, Phys. Rev. C **87**, 014302 (2013), and earlier references therein.

[5] Yu. Ts. Oganessian *et al.*, Phys. Rev. Lett. **109**, 162501 (2012).
[6] Yu. Ts. Oganessian *et al.*, JINR Communication **D7-2002-287** (2002); see http://www.jinr.ru/publish/Preprints/2002/287(D7-2002-287)e.pdf.
[7] Yu. Ts. Oganessian *et al.*, Phys. Rev. C **74**, 044602 (2006).
[8] Niyti, G. Sawhney, M. K. Sharma, and R. K. Gupta, Phys. Rev. C **91**, 054606 (2015).
[9] Yu. Ts. Oganessian *et al.*, Phys. Rev. C **79**, 024603 (2009).
[10] G. Mandaglio, G. Giardina, A. K. Nasirov, and A. Sobiczewski, Phys. Rev. C **86**, 064607 (2012).
[11] T. Cap, K. Siwek-Wilczyńska, M. Kowal, and J. Wilczyński, Phys. Rev. C **88**, 037603 (2013).
[12] N. Wang, E.-G. Zhao, and W. Scheid, Phys. Rev. C **89**, 037601 (2014).
[13] V. Ninov *et al.*, Phys. Rev. Lett. **83**, 1104 (1999).
[14] R. K. Gupta, S. Kumar, R. Kumar, M. Balasubramaniam, and W. Schied, J. Phys. G: Nucl. Part. Phys. **28**, 2875 (2002).
[15] R. Smolańczuk, Phys. Rev. C **56**, 812 (1997); **59**, 2634 (1999); Phys. Rev. Lett. **83**, 4705 (1999).
[16] R. Kumar, K. Sandhu, M. K. Sharma, and R. K. Gupta, Phys. Rev. C **87**, 054610 (2013).
[17] G. Sawhney, K. Sandhu, M. K. Sharma, and R. K. Gupta, Eur. Phys. J. A **50**, 175 (2014).
[18] G. Sawhney, K. Sandhu, M. K. Sharma, and R. K. Gupta, EPJ Web Conf. **86**, 00041 (2015).
[19] R. K. Gupta, in *Clusters in Nuclei*, edited by C. Beck, Lecture Notes in Physics 818 (Springer-Verlag, Berlin, Heidelberg, 2010), Vol. 1, pp. 223–264.
[20] R. K. Gupta, M. Balasubramaniam, R. Kumar, N. Singh, M. Manhas, and W. Greiner, J. Phys. G: Nucl. Part. Phys. **31**, 631 (2005).
[21] J. Blocki, J. Randrup, W. J. Swiatecki, and C. F. Tsang, Ann. Phys. (NY) **105**, 427 (1977).
[22] W. D. Myers and W. J. Swiatecki, Phys. Rev. C **62**, 044610 (2000).
[23] R. K. Gupta, N. Singh, and M. Manhas, Phys. Rev. C **70**, 034608 (2004).
[24] G. Sawhney, A. Kaur, M. K. Sharma, and R. K. Gupta, *Contribution, 75 years of Nuclear Fission: Present status and Future Perspectives, Department of Atomic Energy, BARC Mumbai, May 08–10, 2014*; available at https://inis.iaea.org/search/search.aspx?orig_q=RN:45100417.
[25] G. Sawhney, R. K. Gupta, A. Kaur, and M. K. Sharma, *Extremes of the Nuclear Landscape*, Zakopane Conference on Nuclear Physics, Zakopane, Poland, August 31–September 7, 2014, Book of Abstracts p. 197; available at http://zakopane2014.ifj.edu.pl/download/zakopane_book_of_abstracts.pdf.
[26] S. S. Malik and R. K. Gupta, Phys. Rev. C **39**, 1992 (1989).
[27] S. Kumar and R. K. Gupta, Phys. Rev. C **55**, 218 (1997).
[28] R. K. Gupta, in *Heavy Elements and Related New Phenomena*, edited by W. Greiner and R. K. Gupta (World Scientific, Singapore, 1999), Vol. II, Chap. 18, p. 730.
[29] H. Kröger and W. Scheid, J. Phys. G: Nucl. Part. Phys. **6**, L85 (1980).
[30] N. J. Davidson, S. S. Hsiao, J. Markram, H. G. Miller, and Y. Tzeng, Nucl. Phys. A **570**, 61c (1994).
[31] W. D. Myers and W. J. Swiatecki, Nucl. Phys. A **81**, 1 (1966).
[32] R. Kumar and M. K. Sharma, Phys. Rev. C **85**, 054612 (2012).
[33] K. Sandhu, M. K. Sharma, A. Kaur, and R. K. Gupta, Phys. Rev. C **90**, 034610 (2014).
[34] W. Reisdorf, J. Phys. G: Nucl. Part. Phys. **20**, 1297 (1994).
[35] G. Royer and J. Mignen, J. Phys. G: Nucl. Part. Phys. **18**, 1781 (1992).
[36] H. S. Khosla, S. S. Malik, and R. K. Gupta, Nucl. Phys. A **513**, 115 (1990).
[37] R. K. Gupta, S. Kumar, and W. Scheid, Int. J. Mod. Phys. E **6**, 259 (1997).
[38] T. Matsuse, C. Beck, R. Nouicer, and D. Mahboub, Phys. Rev. C **55**, 1380 (1997).
[39] S. J. Sanders, Phys. Rev. C **44**, 2676 (1991); S. J. Sanders, D. G. Kovar, B. B. Back, C. Beck, D. J. Henderson, R. V. F. Janssens, T. F. Wang, and B. D. Wilkins, *ibid.* **40**, 2091 (1989).
[40] S. K. Arun, R. Kumar, and R. K. Gupta, J. Phys. G: Nucl. Part. Phys. **36**, 085105 (2009).
[41] M. Bansal, S. Chopra, R. K. Gupta, R. Kumar, and M. K. Sharma, Phys. Rev. C **86**, 034604 (2012).
[42] G. Audi, A. H. Wapstra, and C. Thibault, Nucl. Phys. A **729**, 337 (2003).
[43] P. Möller, J. R. Nix, W. D. Myers, and W. J. Swiatecki, At. Data Nucl. Data Tables **59**, 185 (1995).
[44] R. K. Gupta, M. Manhas, and W. Greiner, Phys. Rev. C **73**, 054307 (2006).
[45] Niyti, R. K. Gupta, and W. Greiner, J. Phys. G: Nucl. Part. Phys. **37**, 115103 (2010).
[46] R. K. Gupta, Niyti, M. Manhas, and W. Greiner, J. Phys. G: Nucl. Part. Phys. **36**, 115105 (2009).
[47] S. K. Patra (private communication).
[48] Niyti and R. K. Gupta, Phys. Rev. C **89**, 014603 (2014).
[49] G. M. Carmel Vigila Bai and J. Umai Parvathiy, Pramana J. Phys. **84**, 113 (2015).
[50] K. P. Santhosh and B. Priyanka, Phys. Rev. C **89**, 064604 (2014).
[51] C. Samanta, P. Roy Chowdhury, and D. N. Basu, Nucl. Phys. A **789**, 142 (2007).
[52] G. Royer and H. F. Zhang, Phys. Rev. C **77**, 037602 (2008).
[53] D. N. Poenaru, R. A. Gherghescu, and W. Greiner, Phys. Rev. Lett. **107**, 062503 (2011).
[54] D. N. Poenaru, R. A. Gherghescu, and W. Greiner, Phys. Rev. C **85**, 034615 (2012).